

Synthesis and Characterization of Ultraviolet Light-Emitting Organic Acids

Chun-Ai An · Yanchao Guo · Zhenjun Si · Qian Duan

Received: 28 November 2013 / Accepted: 3 February 2014
© Springer Science+Business Media New York 2014

Abstract Three ultraviolet light-emitting organic acids of 3,3'-(4-phenyl-4H-1,2,4-triazole-3,5-diyl)dibenzoic acid (Tz-1), 4,4',4''-(4H-1,2,4-triazole-3,4,5-triyl)tribenzoic acid (Tz-2), and 4,4'-(4-(4'-carboxy-[1,1'-biphenyl]-4-yl)-4H-1,2,4-triazole-3,5-diyl)dibenzoic acid (Tz-3) were successfully synthesized and fully characterized by the ^1H NMR, the IR absorption spectra, and the X-ray single crystal diffraction. It was found that Tz-1, Tz-2, and Tz-3 could give out the ultraviolet photoluminescent spectra centered at 369 nm, 365 nm and 350 nm, respectively. The luminescence quantum yields of Tz-1 and Tz-2 were measured to be 0.20 and 0.14, respectively. Additionally, the density functional theory (DFT) and the time-dependent DFT calculations were also carried out for Tz-1, Tz-2, and Tz-3.

Keywords Photoluminescence · X-ray single crystal diffraction · Theoretical calculation

Introduction

In the past decades, the studies on the synthesis and the properties of the organic acids [1–12] appealed to many scientific researchers because the organic acids, along with most metal ions, can form diverse metal complexes which are potentially applied in magnetism [1, 2], catalysts [3, 4], sensors [5, 6], luminescence [7–9], etc. In order to further expand the

coverage of the applications, the heteroatoms such as the sulfur atom [10] and the nitrogen atom [2, 11, 12] are often introduced into the organic acids' molecules for these heteroatoms could endow the materials with some special structures and/or excellent properties. For example, the picolinic acid was used to prepare high-efficient organic electroluminescent Ir^{III} complex [7]. Meanwhile, the derivatives of 1,2,4-triazole (Tz-0) [13–15] were widely applied in functional materials because of the fact that these compounds possess the advantages including i) the nitrogen atoms can coordinate to most metal ions, ii) the easy modification of Tz-0 with different functional groups at 3-, 4-, 5- positions would furnish the Tz-0 derivatives with unexpected properties, and iii) the large energy gap of these compounds could endow them with higher-energy light-emitting spectra. Therefore, we designed and synthesized three ultraviolet light-emitting compounds, 3,3'-(4-phenyl-4H-1,2,4-triazole-3,5-diyl)dibenzoic acid (Tz-1), 3,4',3''-(4H-1,2,4-triazole-3,4,5-triyl)tribenzoic acid (Tz-2), and 3,3'-(4-(4'-carboxy-[1,1'-biphenyl]-4-yl)-4H-1,2,4-triazole-3,5-diyl)dibenzoic acid (Tz-3), which were characterized by ^1H NMR, UV–Vis absorption spectra and IR absorption spectra as well as that the crystal structures of Tz-1 and Tz-2 were cultured by the hydrothermal method and correctly resolved. At the same time, the photophysical, the electrochemical, and the theoretical analyses of Tz-1 ~ Tz-3 were also carried out.

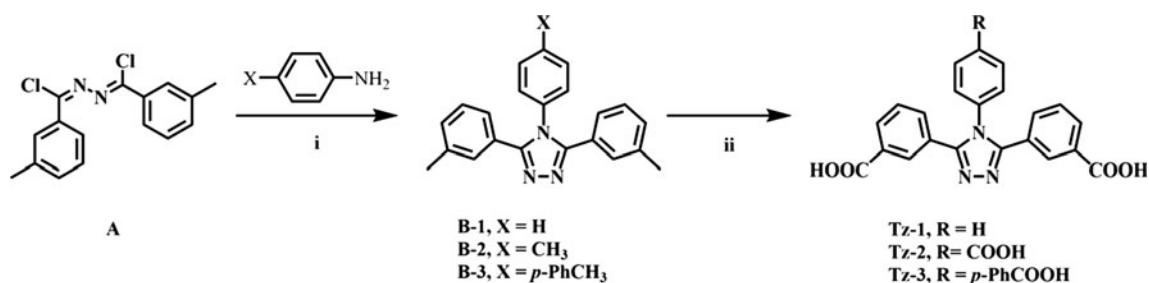
Experimental Section

Materials

N-(chloro(*m*-tolyl)methylene)-3-methylbenzohydrazonoyl chloride (A) were prepared according to the previously reported methods [15]. The solvents used in the synthesis were dried in the standard procedure [16], and all reactions were carried out under nitrogen using Schlenk techniques.

Electronic supplementary material The online version of this article (doi:10.1007/s10895-014-1362-7) contains supplementary material, which is available to authorized users.

C.-A. An · Y. Guo · Z. Si (✉) · Q. Duan (✉)
School of Materials Science and Engineering, Changchun University of Science and Technology, Changchun 130022, People's Republic of China
e-mail: szj@cust.edu.cn
e-mail: duanqian88@hotmail.com



Scheme 1 Synthetic route to Tz-1 ~ Tz-3. i) N,N-dimethylaniline, 145 °C, 24 h; ii) NaOH, KMnO₄, H₂O, reflux, 12 h

Synthesis of Tz-1

The mixture of A (7.5 g, 24.590 mmol), aniline (2.3 mL, 25.190 mmol) and N,N-Dimethylaniline (45.0 mL) were added into a 250.0 mL flask equipped with a magnetic stirrer and reflux condenser and reacted 36 h at 145 °C. After being cooled to the room temperature, diluted hydrochloric acid (10 %, 80.0 mL) was added into the mixture and stirred for another 2 h, then the white solid was filtered and washed with the diluted hydrochloric acid (10 %, 50.0 mL × 3) and pure water successively, and then dried 12 h in vacuum at 30 °C to give pure 4-phenyl-3,5-di-*m*-tolyl-4H-1,2,4-triazole (B-1) in yield of ca. 60 %. The mixture of B-1 (3.25 g, 10.000 mmol), KMnO₄ (12.64 g, 80.000 mmol) and NaOH (8.13 g, 0.203 mol) were added into a 250.0 mL round-bottomed flask

containing 120.0 mL distilled water and 20.0 mL pyridine and heated up to 100 °C for 12 h and then cooled to room temperature, 30.0 mL ethanol was added into the mixture which was stirred for another 0.5 h, then the solid was filtered. The filtrate was acidified with the diluted HCl aqueous (10 %) to pH=3. The precipitated Tz-1 was obtained in yield of ca. 75 % by filtration. ¹H NMR (400 MHz, DMSO-*d*₆): δ=13.08 (s, 2H), 8.05–7.45 (d, 13H); IR (KBr)/cm⁻¹: 3,500, 3,073, 2,923, 2,614, 1,926, 1,695, 1,612, 1,495.

Synthesis of Tz-2

The synthesis of Tz-2 was similar to that of Tz-1 by replacing aniline with *p*-toluidine. Yield in total was 41.2 %. ¹H NMR (400 MHz, DMSO-*d*₆): δ=13.18 (s, 3H), 8.07–7.96 (m, 6H); 7.60 (d, *J*=8Hz, 4H); 7.51 (t, *J*=8 Hz, 2H); IR (KBr)/cm⁻¹: 3,419, 2,902, 2,615, 1,724, 1,606, 1,512, 1,461, 1,254.

Synthesis of Tz-3

The synthesis of Tz-3 was similar to that of Tz-1 by replacing aniline with 4'-methyl-[1,1'-biphenyl]-4-amine. Yield in total

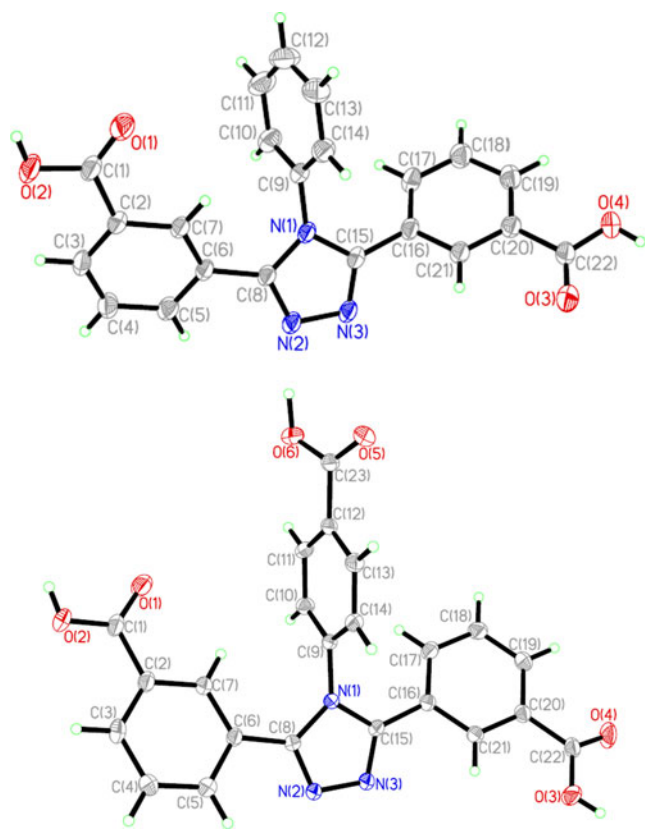


Fig. 1 ORTEP drawings of Tz-1 (upper) and Tz-2 (lower) with 30 % thermal ellipsoids

Table 1 Crystalline data of Tz-1 and Tz-2

| | Tz-1 | Tz-2 |
|----------------------------|---|---|
| Empirical formula | C ₂₂ H ₁₇ N ₃ O ₅ | C ₂₃ H ₁₅ N ₃ O ₆ |
| Formula weight | 403.39 | 429.38 |
| CCDC no. | 935,264 | 956,492 |
| Crystal system | Monoclinic | Monoclinic |
| Space group | <i>P</i> 2 ₁ / <i>n</i> | <i>P</i> 2 ₁ / <i>c</i> |
| <i>a</i> (Å) | 12.038(2) | 8.0474(16) |
| <i>b</i> (Å) | 10.620(2) | 18.379(4) |
| <i>c</i> (Å) | 15.528(3) | 13.095(3) |
| α (°) | 90.000 | 90 |
| β (°) | 91.71(3) | 96.48 |
| γ (°) | 90.000 | 90 |
| <i>V</i> (Å ³) | 1984.3(7) | 1924.4(7) |
| <i>z</i> | 4 | 4 |
| μ (mm ⁻¹) | 0.098 | 0.110 |
| <i>F</i> (000) | 840 | 888 |

Table 2 Selective bond distances (Å) and bond angles (°) of Tz-1 and Tz-2

| | Tz-1 | Tz-2 |
|-------------------|------------|------------|
| C(6)-C(8) | 1.472(3) | 1.475(3) |
| C(8)-N(2) | 1.309(2) | 1.314(2) |
| C(8)-N(1) | 1.378(2) | 1.376(3) |
| C(9)-N(1) | 1.440(2) | 1.445(3) |
| C(15)-N(3) | 1.309(3) | 1.313(3) |
| C(15)-N(1) | 1.370(3) | 1.379(2) |
| C(15)-C(16) | 1.478(3) | 1.470(3) |
| N(2)-N(3) | 1.385(2) | 1.381(2) |
| C(7)-C(6)-C(8) | 123.00(17) | 123.09(19) |
| C(5)-C(6)-C(8) | 117.89(18) | 118.07(19) |
| N(2)-C(8)-N(1) | 109.01(16) | 109.18(17) |
| N(2)-C(8)-C(6) | 124.26(17) | 123.18(18) |
| N(1)-C(8)-C(6) | 126.72(17) | 127.60(18) |
| C(14)-C(9)-N(1) | 119.22(18) | 118.69(17) |
| C(10)-C(9)-N(1) | 119.54(18) | 119.63(18) |
| N(3)-C(15)-N(1) | 109.77(16) | 109.26(18) |
| N(3)-C(15)-C(16) | 124.99(19) | 124.22(18) |
| N(1)-C(15)-C(16) | 125.24(17) | 126.50(18) |
| C(21)-C(16)-C(15) | 118.99(18) | 117.46(19) |
| C(17)-C(16)-C(15) | 121.46(19) | 123.87(19) |

was 38.4 %. ¹H NMR (400 MHz, DMSO-d₆): δ=13.08 (s, 3H); 8.03 (t, *J*=10 Hz, 4H); 7.97 (d, *J*=8Hz, 2H); 7.87 (m, *J*=8Hz, 4H); 7.68(d, *J*=8 Hz, 2H); 7.62(d, *J*=8 Hz, 2H); 7.52 (t, *J*=8 Hz, 2H) IR (KBr)/cm⁻¹: 3,288, 2,879, 2,553, 1,685, 1,610, 1,523, 1,425, 1,284.

Measurements

The IR spectra was acquired using a FTIR-8400S SHIMADZU spectrophotometer in the 4,000–400 cm⁻¹ region with KBr pellets. The UV-Vis absorption and photoluminescent (PL) spectra of methanol solutions with ca. 10⁻⁴ mol/L samples were recorded on a Perkin Elmer Lambda 900 UV/Vis/NIR spectrophotometer and a SHIMADZU RF-5301 PC spectrofluorophotometer, respectively. The luminescence quantum yields (LQYs) were measured by comparing fluorescence intensities

Table 3 Hydrogen bond distances (Å) in Tz-1 and Tz-2

| Tz-1 | Tz-2 |
|-----------------|-------|
| O(3)-H(5B)-O(5) | 2.874 |
| O(4)-H(4A)-O(5) | 2.553 |
| N(2)-H(5A)-O(5) | 2.793 |
| N(3)-H(2A)-O(2) | 2.760 |
| O(1)-H(2)-O(2) | 2.622 |
| N(2)-H(6A)-O(6) | 2.689 |
| N(3)-H(3A)-O(3) | 2.783 |

(integrated areas) of a standard sample (quinine sulfate) and the unknown sample according to Eq. 1.

$$\Phi_{\text{unk}} = \Phi_{\text{std}}(I_{\text{unk}}/A_{\text{unk}})(A_{\text{std}}/I_{\text{std}})(\eta_{\text{unk}}/\eta_{\text{std}})^2 \quad (1)$$

where Φ_{unk} is the LQY of the unknown sample; Φ_{std} is the LQY of quinine sulfate and taken as 0.546 [17]; I_{unk} and I_{std} are the integrated fluorescence intensities of the unknown sample and quinine sulfate at corresponding excitation wavelength, respectively; A_{unk} and A_{std} are the absorbances of the unknown sample and quinine sulphate at the corresponding excitation wavelengths, respectively. The η_{unk} and η_{std} are the refractive indices of the corresponding solvents (pure solvents were assumed). ¹H NMR spectra was obtained using a Bruker AVANVE 400 MHz spectrometer with tetramethylsilane as the internal standard. The crystal structures of Tz-1 and Tz-2 were measured on a Bruker Smart Apex CCD single-crystal diffractometer using λ (Mo Kα) radiation, 0.7107 Å at 293 K and solved using the SHELXL-97 program [18–20]. The cyclic voltammetry measurements were conducted on a CHI825D electrochemical workstation with a polished Pt plate as the working electrode, Pt mesh as the counter electrode, and a commercially available saturated calomel electrode (SCE) as the reference electrode, at a scan rate of 0.1 V/s. The voltammograms were recorded using CH₃CN/DMSO (v/v=10/1) solutions with ~ 10⁻³ M sample and 0.1 M tetrabutylammonium hexafluorophosphate (TBAPF₆) as the supporting electrolyte. Prior to each electrochemical measurement, the solution was purged with nitrogen for ~10–15 min to remove the dissolved O₂ gas.

Computational Details

The geometrical structures of the ground states were optimized at b3lyp/6-31 g* level [21] in gas phase by the density functional theory (DFT) [22]. On the basis of the optimized ground state geometry structures, the absorption spectral properties in methanol media were calculated by time-dependent DFT (TDDFT) method [23–25] associated with the polarized continuum model (PCM) [26] in methanol media. All the calculations were performed with the Gaussian 09 package [27].

Results and Discussion

Molecular Structures

As presented in Scheme 1, the B-1, 3,5-di-m-tolyl-4-(p-tolyl)-4H-1,2,4-triazole (B-2) and 4-(4'-methyl-[1,1'-biphenyl]-4-yl)-3,5-di-m-tolyl-4H-1,2,4-triazole (B-3) were prepared from the precursors of A and aniline derivatives in N,N-Dimethylaniline at 145 °C, and then converted into the target compounds of Tz-1 ~ Tz-3 in hot KMnO₄/NaOH aqueous

Fig. 2 Single-layer (a) and double-layer (b) 2D supermolecular structures of Tz-1

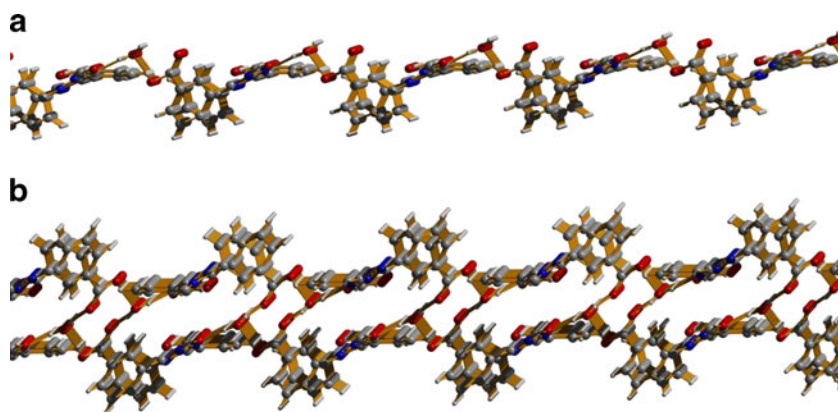
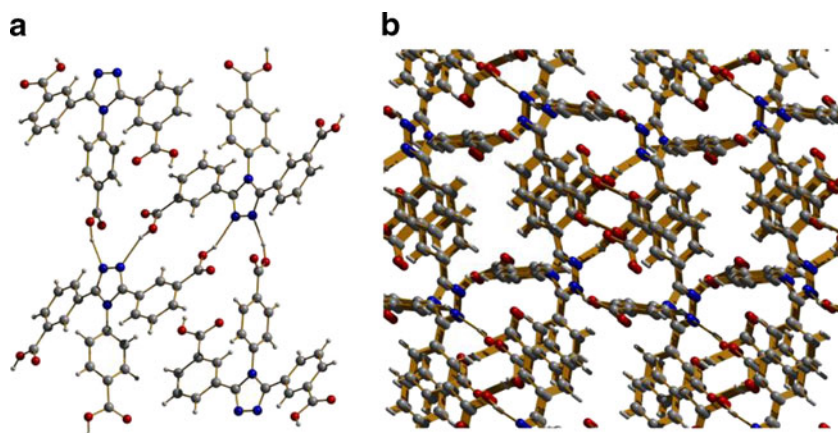


Fig. 3 Intermolecular hydrogen bond interactions between 1,2,4-triazole moiety and the acid group(A) and the 3D supermolecular structure of Tz-2



solution. The monoclinic crystals of Tz-1 with space group of $P2_1/n$ and Tz-2 with space group of $P2_1/c$ were cultured by the hydrothermal methods. The corresponding ellipsoid crystal structures of Tz-1 and Tz-2 were prepared in 30 % thermal ellipsoids and presented in Fig. 1. The crystal data and the selective bond distances and angles are listed in Tables 1 and 2, respectively, while intermolecular hydrogen bond interactions (IHBI) are listed in Table 3.

The dihedral angles between the Tz-0 moiety and the phenyl groups on 3-, 4-, 5-positions of the Tz-0 moiety were measured to be $44.640(59)^\circ$, $70.655(53)^\circ$, and $28.365(54)^\circ$ for Tz-1, and $28.884(41)^\circ$, $84.118(57)^\circ$ and $21.887(43)^\circ$ for Tz-2, respectively. These data suggest that the π -conjunction between 3- (or 5-) aryl groups and the Tz-0 moiety should be better than that between 4-aryl group and the Tz-0 moiety as well as that the size of the 4-aryl group could greatly affect the π -conjunction interaction between 4-aryl groups and Tz-0 moiety. In Tz-1, the bond distance (d) of IHBI of $N(2)\cdots H(5A)-O(5)$, $N(3)\cdots H(2A)-O(2)$, and $O(5)\cdots H(4A)-O(4)$ are 2.793 Å, 2.760 Å, and 2.553 Å, respectively. These IHBI connect Tz-1 molecules to be the single-layer based 2D supermolecules (Fig. 2a). These single-layer based 2D supermolecules further expand to the

double-layer based 2D supermolecules (Fig. 2b) with the help of the IHBI of $O(3)\cdots H(5B)-O(5)$ ($d=2.874$ Å). After adding another carboxylic group, in Tz-2, The IHBI of $N(2)\cdots H(6A)-O(6)$ with d of 2.689 Å and $N(3)\cdots H(3A)-O(3)$ with d of 2.783 Å connect Tz-2 molecules to be the 2D supermolecules (Fig. 3a) which are further

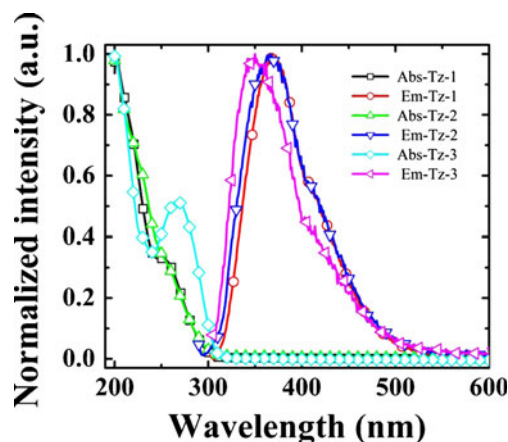


Fig. 4 UV-Vis absorption spectra (Abs) and the emission spectrum (Em) of Tz-1 ~ Tz-3 in methanol at room temperature

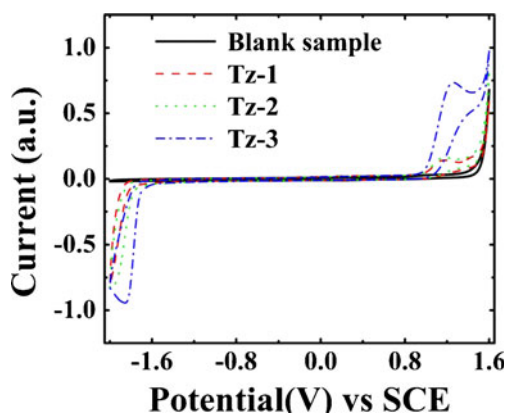


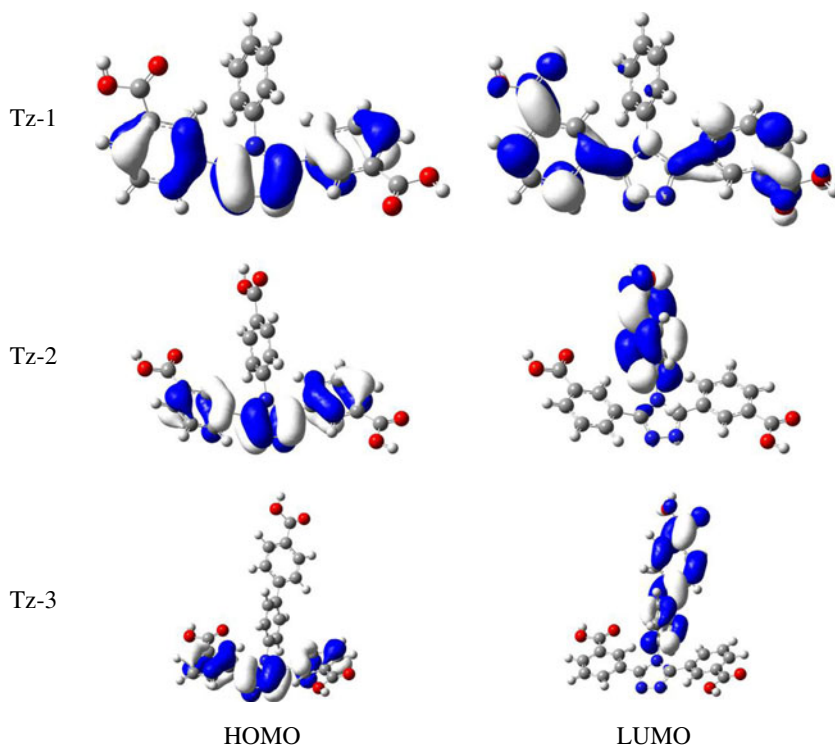
Fig. 5 Electrochemistry of Tz-1 ~Tz-3 in CH₃CN/DMSO (v/v=10:1) solution with 0.1 M TBAPF₆ as the supporting electrolyte

connected to be 3D supermolecules by the IHBI of O(1)···H(2)–O(2) ($d=2.622$ Å) (Fig. 3b).

Photophysical Properties

The UV–Vis absorption spectra and the emission spectra of Tz-1 ~ Tz-3 are presented in Fig. 4. According to the previous reports [13] and the theoretical analysis (vide infra), the absorption band peaked at ~ 200 nm should be mainly attributed to the $\pi \rightarrow \pi^*$ transitions and the shoulder band in the range 240 ~ 320 nm should be assigned to the contribution of the intramolecular charge transfer (ICT) transitions and the $\pi \rightarrow \pi^*$ transitions. Upon the UV excitation, Tz-1, Tz-2 and Tz-3 give out in their ethanol solutions the ultraviolet PL spectra

Fig. 6 Electron density plots of the HOMO and LUMO of Tz-1 ~ Tz-3 in gas phase at DFT/B3LYP/6-31G* level



peaked at 369 nm with full width at half maximum (HWHM) of ca. 81 nm, 366 nm with HWHM of 44.5 nm, 350 nm with HWHM of 38 nm, respectively. The LQYs of Tz-1, Tz-2 and Tz-3 were measured reference to the quinine sulfate (LQY= 0.546) to be 0.20, 0.14, and 0.06, respectively, the higher LQYs of Tz-1 and Tz-2 should be partially attributed to their inflexible molecular structures [28].

Electrochemistry

In order to investigate the distribution of the frontier molecular orbitals, the electrochemical properties of Tz-1 ~ Tz-3 are studied in CH₃CN/DMSO (v/v=10:1) solution through cyclic voltammetry using TBAPF₆ as the supporting electrolyte (Fig. 5). The irreversible anodic waves peak at +1.18 V with an onset oxidation ($V_{\text{onset}}(\text{OX})$) of +0.98 V for Tz-1, +1.16 V with $V_{\text{onset}}(\text{OX})$ of +0.98 V for Tz-2, and +1.26 V with $V_{\text{onset}}(\text{OX})$ of +1.01 V for Tz-3, respectively. The energies of the highest occupied molecular orbital (E_{HOMO}) are obtained according to the following equation: $E_{\text{HOMO}}=[V_{\text{SCE}} - V_{\text{onset}}(\text{OX})]$ eV [17], where the V_{SCE} is the electrode potential of the SCE which should be –4.74 eV in a vacuum, and the values of E_{HOMO} of Tz-1, Tz-2, and Tz-3 are calculated to be –5.72 eV, –5.72 eV, and –5.75 eV, respectively. At the same time, the values for the energy of the lowest unoccupied molecular orbital (E_{LUMO}) are calculated with the equation of $E_{\text{LUMO}}=[V_{\text{SCE}} - V_{\text{onset}}(\text{Red})]$ eV [17], where the $V_{\text{onset}}(\text{Red})$ is the onset reduction potential which should be –1.83 V, –1.78 V, and –1.72 V for Tz-1, Tz-2, and Tz-3, respectively.

Therefore, the values of the E_{LUMO} should be -2.91 eV, -2.96 eV, and -3.02 eV, respectively, and the energy gap (ΔE) between HOMO and LUMO of Tz-1 ~ Tz-3 should be 2.81 eV, 2.76 eV, and 2.73 eV, respectively. These results present the fact that the E_{LUMO} and ΔE of Tz-1 ~ Tz-3 are in the order of Tz-1 > Tz-2 > Tz-3, which is in accordance with the theoretical studies (vide infra). It is also found that the ΔE s of Tz-2 ~ Tz-3 are higher than that of the triplet energy gape of the typical blue triplet emitter of Firpic (2.62 eV) [29], which suggests that Tz-1 ~ Tz-3 might be used as the host materials of the blue phosphorescent light-emitting devices.

Theoretical Calculations

Simulation on the Ground State Molecules

According to the optimized ground-state molecular structures of Tz-1 ~ Tz-3 (Fig. 6), the dihedral angles between the Tz-0 moiety and the phenyl groups on its 3-, 4-, 5-positions were simulated to be 33.31° , 69.56° , and 29.61° for Tz-1, 29.34° , 80.37° and 26.32° for Tz-2, and 28.51° , 93.11° , and 24.01° for Tz-3, respectively. These data indicate that the π -conjunction between the Tz-0 moiety and the aryl group on its 4-position should be in the following order: Tz-1 > Tz-2 > Tz-3, that is, the increase of the size of aryl group on 4-position of Tz-0 moiety could weaken the π -conjunction, which is consistent with the fact that the peaks of the PL spectra of Tz-1 ~ Tz-3 locates at 369 nm, 366 nm, and 350 nm, respectively [30, 31].

The distributions of the simulated HOMOs and LUMOs of Tz-1 ~ Tz-3 are presented in Fig. S1 ~ S3, respectively, while the compositions of the simulated frontier molecular orbitals of Tz-1 ~ Tz-3 are listed in Table 4. The HOMO of Tz-1 is composed of the π orbitals of Tz-0 moiety with 52.3 % contributions and 3- and 5-PhCOOH moieties with 47.3 % contributions. The LUMO of the Tz-1 is mainly contributed by the π^* orbitals on 3- and 5-PhCOOH moieties with 86.6 % contributions. The HOMO of Tz-2 (Tz-3), similar to that of Tz-1, is composed of the π orbitals of Tz-0 moiety with 50.5 % (50.8 %) contributions and 3-/5-PhCOOH groups attached to Tz-0 moiety with 49.4 % (49.0 %) contributions, while the LUMO of Tz-2 (Tz-3) is comprised with the π^* orbitals on the 4-PhCOOH (4-Ph₂COOH) group with 89.2 % (94.7 %) contributions. These data suggest that the composition of LUMOs of the derivatives of Tz-0 can be more obviously affected by the groups attached to their 4-position than that of their HOMOs. At the same time, the E_{HOMOs} and the E_{LUMOs} are calculated to be -6.14 eV and -1.57 eV for Tz-1, -6.23 eV and -1.67 eV for Tz-2, and -6.16 eV and -1.63 eV for Tz-3, respectively. Therefore, the ΔE are calculated to be 4.57 , 4.23 , and 4.19 eV for Tz-1, Tz-2, and Tz-3, respectively, which are bigger than those from the experimental measurements. But the values of these theoretically calculated data and the above mentioned electrochemically

Table 4 Frontier molecular orbital compositions (%) of Tz-1 ~ Tz-3 calculated in the gas phase at the DFT/B3LYP/6-31 g* level

| Orbital | $E(\text{eV})$ | Distribution (%) | | |
|-------------|----------------|-------------------------|------|------------------|
| | | 3- and 5-R ₁ | Tz-0 | 4-R ₂ |
| Tz-1 | | | | |
| L+3 | -0.79 | | | 84.9 |
| L+2 | -1.13 | 76.1 | 21.5 | |
| L+1 | -1.42 | 91.6 | | |
| L | -1.57 | 86.6 | | |
| ΔE | 4.57 | | | |
| H | -6.14 | 47.3 | 52.3 | |
| H-1 | -6.73 | | 83.9 | |
| H-2 | -7.15 | 66.0 | | 19.7 |
| H-3 | -7.20 | 89.2 | | |
| Tz-2 | | | | |
| L+3 | -1.19 | 70.7 | | |
| L+2 | -1.51 | 90.6 | | |
| L+1 | -1.67 | 82.1 | | |
| L | -2.00 | | | 89.2 |
| ΔE | 4.23 | | | |
| H | -6.23 | 49.4 | 50.5 | |
| H-1 | -6.91 | | 86.3 | |
| H-2 | -7.31 | 95.6 | | |
| H-3 | -7.34 | 97.5 | | |
| Tz-3 | | | | |
| L+3 | -1.17 | 68.7 | | |
| L+2 | -1.47 | 90.9 | | |
| L+1 | -1.63 | 83.5 | | |
| L | -1.97 | | | 94.7 |
| ΔE | 4.19 | | | |
| H | -6.16 | 49.0 | 50.8 | |
| H-1 | -6.67 | | 50.6 | 44.0 |
| H-2 | -7.08 | | 59.3 | 29.0 |
| H-3 | -7.29 | 94.3 | | |

R₁ = -PhCOOH, R₂ = -Ph for Tz-1, -PhCOOH for Tz-2, and -Ph₂COOH for Tz-3, respectively

measured data are in the same changing trend. The difference between the experimental measurements and the theoretical calculations should be mainly attributed to the ignorance of the solution effect during the optimization of the geometrical structures of Tz-1 ~ Tz-3.

UV-Vis Absorption Spectra

As presented in Table 5, the lowest lying singlet → singlet absorptions with the configurations of HOMO → LUMO are calculated at 299 and 322 , and 312 nm for Tz-1, Tz-2, and Tz-3, respectively, which means that the lowest lying transitions should be described as the $\pi \rightarrow \pi^*$ and the intramolecular

Table 5 Calculated absorption of Tz-1 ~ Tz-3 in methanol media according to the TDDFT/B3LYP/6-31 g* calculations

| State | Transition (%) | E (eV)/λ (nm) | Osc. strength | Assign |
|-------|----------------|---------------|---------------|----------|
| Tz-1 | | | | |
| 1 | H→L (94) | 4.14/299 | 0.3142 | ICT/π→π* |
| 3 | H→L+2 (90) | 4.50/276 | 0.4873 | ICT/π→π* |
| 11 | H-3→L (46) | 5.04/246 | 0.1378 | π→π* |
| 21 | H-5→L+1 (64) | 5.47/226 | 0.1906 | ICT/π→π* |
| 44 | H-10→L+1 (20) | 6.28/197 | 0.1027 | π→π* |
| Tz-2 | | | | |
| 1 | H→L (99) | 3.85/322 | 0.0025 | ICT |
| 2 | H→L+1 (95) | 4.14/299 | 0.4534 | ICT/π→π* |
| 4 | H→L+3 (88) | 4.48/277 | 0.4457 | ICT/π→π* |
| 17 | H-3→L+1 (38) | | | |
| | H-4→L+2 (38) | 5.09/244 | 0.1922 | ICT/π→π* |
| 30 | H-9→L (20) | 5.58/222 | 0.1846 | ICT/π→π* |
| Tz-3 | | | | |
| 1 | H→L (96) | 3.98/312 | 0.0131 | ICT |
| 2 | H→L+1 (94) | 4.11/301 | 0.4181 | ICT/π→π* |
| 4 | H-1→L (84) | 4.36/284 | 0.6622 | ICT/π→π* |
| 6 | H→L+3 (86) | 4.45/278 | 0.4658 | ICT/π→π* |
| 19 | H-4→L+1 (28) | 5.08/244 | 0.1439 | π→π* |

charge transfer (ICT) based on the $\pi(\text{Tz-0} + 3\text{-/5-PhCOOH}) \rightarrow \pi^*(3\text{-/5-PhCOOH})$ transitions for Tz-1, the ICT based on the $\pi(\text{Tz-0} + 3\text{-/5-PhCOOH}) \rightarrow \pi^*(4\text{-PhCOOH})$ transfer for Tz-2 and the ICT based on the $\pi(\text{Tz-0} + 3\text{-/5-PhCOOH}) \rightarrow \pi^*(4\text{-PhPhCOOH})$ transfer for Tz-3, respectively.

The absorptions with the largest oscillator strengths are simulated to be at 276 nm with the configuration of HOMO → LUMO + 2 for Tz-1, 299 nm with the configuration of HOMO → LUMO + 1 for Tz-2, and 284 nm with the configuration of HOMO-1 → LUMO for Tz-3, respectively. According to the fact that the LUMO + 2 of Tz-1, the LUMO + 1 of Tz-2, and the HOMO-1 of Tz-3 are mainly comprised of the $\pi^*(3\text{-/5-PhCOOH} + \text{Tz-0})$, $\pi^*(3\text{-/5-PhCOOH})$, and $\pi(4\text{-Ph}_2\text{COOH} + \text{Tz-0})$ (Table 4), respectively, these largest oscillator strengths based absorption should be with the character of $\pi \rightarrow \pi^*/\text{ICT}$ transitions. At the same time, the absorptions with the moderate oscillator of Tz-1 ~ Tz-3 are calculated to be the mixture transitions of the $\pi \rightarrow \pi^*/\text{ICT}$ transitions.

Conclusion

In summary, the synthesis and the characterization of the UV light-emitting organic acids of Tz-1 ~ Tz-3 are reported in this article. The PL spectra of Tz-1 ~ Tz-3 centered at 369 nm, 365 nm, and 350 nm, respectively, which is consistent with the theoretically simulated order (Tz-1 > Tz-2 > Tz-3) of the π -conjunction strength between the Tz-0 moiety and the aryl group on its 4-position. The LQYs of Tz-1 and Tz-2 are 0.20

and 0.14, respectively. Therefore, the titled organic acids Tz-1 ~ Tz-3 could be used as the host materials in blue phosphorescent light-emitting devices.

Acknowledgments The authors are grateful to financial aid from the National Natural Science Foundation of China (Grant No. 21271033).

References

- Sanchiz J, Pasán J, Fabelo O, Lloret F, Julve M, Ruiz-Pérez C (2010) $[\text{Cu}_3(\text{Hmesox})_3]^{3-}$: a precursor for the rational design of chiral molecule-based magnets (Hmesox = 2-dihydroxymalonic acid). *Inorg Chem* 49:7880–7889
- Li X, Wu B, Wang R, Zhang H, Niu C, Niu Y, Hou H (2010) Hierarchical assembly of extended coordination networks constructed by novel metallacalix[4]arenes building blocks. *Inorg Chem* 49:2600–2613
- Brunelli NA, Venkatasubbaiah K, Jones CW (2012) Cooperative catalysis with acid–base bifunctional mesoporous silica: impact of grafting and co-condensation synthesis methods on material structure and catalytic properties. *Chem Mater* 24:2433–2442
- Torrado A, Imperiali B (1996) New synthetic amino acids for the design and synthesis of peptide-based metal ion sensors. *J Org Chem* 61:8940–8948
- Joanna O, Roman P (2013) The performance of 7-hydroxycoumarin-3-carbonitrile and 7-hydroxycoumarin-3-carboxylic acid as fluorescent probes for monitoring of cationic photopolymerization processes by FPT. *J Appl Polym Sci* 128:1974–1978
- Laurenti M, Blanco FG, Lopez-Cabarcos E, Rubio-Retama J (2013) Detection of heavy metal ions using a water-soluble conjugated polymer based on thiophene and meso-2,3-dimercaptosuccinic acid. *Polym Int* 62:811–816

7. Adachi C, Kwong RC, Djurovich P, Adamovich V, Baldo MA, Thompson ME, Forrest SR (2001) Endothermic energy transfer: a mechanism for generating very efficient high-energy phosphorescent emission in organic materials. *Appl Phys Lett* 79:2082–2084
8. Jou J, Hsu M, Wang W, Shen S, Wu M, Chen S, Chen H (2009) Solution-processable, high-molecule-based trifluoromethyl-iridium complex for extraordinarily high efficiency blue-green organic light-emitting diode. *Chem Mater* 21:2565–2567
9. Brown-Xu SE, Chisholm MH, Durr CB, Silker TF (2013) Metal-metal quadruple bonds supported by 5-ethynylthiophene-2-carboxylato ligands: preparation, molecular and electronic structures, photoexcited state dynamics, and application as molecular synthons. *J Am Chem Soc* 135:8254–8259
10. Saha A, Latif IA, Datta SN (2011) Photoswitching magnetic cross-over in organic molecular systems. *J Phys Chem A* 115:1371–1379
11. Aijaz A, Sanudo EC, Bharadwaj PK (2011) Construction of coordination polymers with a bifurcating ligand: synthesis, structure, photoluminescence, and magnetic studies. *Cryst Growth Des* 11: 1122–1134
12. Guo Y, Shi T, Si Z, Duan Q, Shi L (2013) Novel magnetic Co^{II} complexes: synthesis and characterization. *Inorg Chem Commun* 34: 15–18
13. Kim JH, Yoon DY, Kim JW, Kim JJ (2007) New host materials with high triplet energy level for blue-emitting electrophosphorescent device. *Synth Met* 157:743–750
14. Hiroko N, Sachiko K, Nobuharu O, Satoshi S (2008) Triazole derivative, and light-emitting device, and electronic device with the use of triazole derivative. U.S. Pat Appl Publ US20080286607A1
15. Li J, Mi X, Wan Y, Si Z, Sun H, Duan Q, He X, Yan D, Wan S (2012) Synthesis, measurements, and theoretical analysis of carbazole derivatives with high-triplet-energy. *J Lumin* 132:1200–1206
16. Armarego WLE, Chai CLL (2003) Purification of laboratory chemicals, 5th edn. Elsevier Science, Burlington
17. Ye K, Wang J, Sun H, Liu Y, Mu Z, Li F, Jiang S, Zhang J, Zhang H, Wang Y, Che CM (2005) Supramolecular structures and assembly and luminescent properties of quinacridone derivatives. *J Phys Chem B* 109:8008–8016
18. Sheldrick GM (1998) SHELXTL. Version 5.10. Siemens analytical X-ray instruments Inc, Madison
19. Bruker (1995) AXS SMART and SAINT. Siemens analytical X-ray instruments Inc, Madison
20. Sheldrick GM (1996) SADABS. University of Göttingen, Göttingen
21. Igor A, Payam M, Jérôme C, Luisa CD (2007) Influence of substituents on the energy and nature of the lowest excited states of heteroleptic phosphorescent Ir(III) complexes: a joint theoretical and experimental study. *J Am Chem Soc* 129:8247–8258
22. Runge E, Gross EKV (1984) Density-functional theory for time-dependent systems. *Phys Rev Lett* 52:997–1000
23. Autschbach J, Ziegler T, Gisbergen SJA, Baerends EJ (2002) Chiroptical properties from time-dependent density functional theory. I. Circular dichroism spectra of organic molecules. *J Chem Phys* 116:6930–6940
24. Helgaker T, Jørgensen P (1991) An electronic hamiltonian for origin independent calculations of magnetic properties. *J Chem Phys* 95: 2595–2601
25. Bak KL, Jørgensen P, Helgaker T, Rund K, Jensen HJA (1993) Gauge-origin independent multiconfigurational self-consistent-field theory for vibrational circular dichroism. *J Chem Phys* 98:8873–8887
26. Mennucci B, Tomasi J (1997) Continuum solvation models: a new approach to the problem of solute's charge distribution and cavity boundaries. *J Chem Phys* 106:5151–5158
27. Frisch MJ, Trucks GW, Schlegel HB, Scuseria GE, Robb MA, Cheeseman JR, Scalmani G, Barone V, Mennucci B, Petersson GA, Nakatsuji H, Caricato M, Li X, Hratchian HP, Izmaylov AF, Bloino J, Zheng G, Sonnenberg JL, Hada M, Ehara M, Toyota K, Fukuda R, Hasegawa J, Ishida M, Nakajima T, Honda Y, Kitao O, Nakai H, Vreven T, Montgomery JA Jr, Peralta JE, Ogliaro F, Bearpark M, Heyd JJ, Brothers E, Kudin KN, Staroverov VN, Kobayashi R, Normand J, Raghavachari K, Rendell A, Burant JC, Iyengar SS, Tomasi J, Cossi M, Rega N, Millam JM, Klene M, Knox JE, Cross JB, Bakken V, Adamo C, Jaramillo J, Gomperts R, Stratmann RE, Yazyev O, Austin AJ, Cammi R, Pomelli C, Ochterski JW, Martin RL, Morokuma K, Zakrzewski VG, Voth GA, Salvador P, Dannenberg JJ, Dapprich S, Daniels AD, Farkas O, Foresman JB, Ortiz JV, Cioslowski J, Fox DJ (2009) Gaussian 09 revision D.01. Gaussian Inc, Wallingford
28. Tao Y, Wang Q, Yang C, Wang Q, Zhang Z, Zou T, Qin J, Ma D (2008) A simple carbazole/oxadiazole hybrid molecule: an excellent bipolar host for green and red phosphorescent OLEDs. *Angew Chem Int Ed* 47:8104–8107
29. Hsu FM, Chien CH, Shu CF, Lai CH, Hsieh CC, Wang KW, Chou PT (2009) A bipolar host material containing triphenylamine and diphenylphosphoryl-substituted fluorene units for highly efficient blue electrophosphorescence. *Adv Funct Mater* 19:2834–2843
30. Hu JY, Feng X, Seto N, Do JH, Zeng X, Tao Z, Yamato T (2013) Synthesis, structural and spectral properties of diarylamino-functionalized pyrene derivatives via Buchwald–Hartwig amination reaction. *J Mol Struct* 1035:19–26
31. He J, Liu H, Dai Y, Ou X, Wang J, Tao S, Zhang X, Wang P, Ma D (2009) Nonconjugated carbazoles: a series of novel host materials for highly efficient blue electrophosphorescent OLEDs. *J Phys Chem C* 113:6761–6767